

Full range spectral domain optical coherence tomography using a fiber-optic probe as a self-phase shifter

Eun Jung Min,¹ Jun Geun Shin,¹ Jae Hwi Lee,¹ Yoshiaki Yasuno,² and Byeong Ha Lee^{1,*}

¹*School of Information and Communications, Gwangju Institute of Science and Technology, 261 Cheomdan-gwagiro, Buk-gu, Gwangju 500-712, South Korea*

²*Institute of Applied Physics, University of Tsukuba, Tennôdai 1-1-1, Tsukuba, Ibaraki 305-8573, Japan*

*Corresponding author: leebh@gist.ac.kr

Received March 21, 2012; revised May 16, 2012; accepted May 21, 2012;
posted May 25, 2012 (Doc. ID 165186); published July 19, 2012

We present a full range handheld probe type spectral domain optical coherence tomography (SD-OCT) method. Here, the sample arm is composed of a tilted fiber-optic cantilever scanner; thus, the phase shift concurrently occurs while sample scanning. With the phase shift, we could achieve a full range complex-conjugate-free OCT image with no additional phase shifters in the reference arm. To realize this technique, a magnetically actuated probe was adopted. Full range SD-OCT images of a pearl, human fingernail, and human tooth were subsequently obtained using this suggested probe. The scanning range and acquisition speed were 3 mm and 20 frames/s, respectively. © 2012 Optical Society of America

OCIS codes: 110.2350, 110.4500, 100.0100, 120.5800.

Optical coherence tomography (OCT) [1] is a powerful noninvasive imaging modality that is used to provide high resolution tomographic imaging. In particular, due to its improved sensitivity and dynamic range compared with time domain OCT, spectral domain OCT (SD-OCT) [2] has been developed. In addition, OCT systems based on fiber-optic endoscopic and handheld probes [3–5] have become a popular area of research, because of advantages such as compactness, flexibility, low insertion loss, alignment-free, and high speed scanning. Even with these advantages, however, SD-OCT systems have inherent problems during signal processing. For example, the reconstructed image is symmetrical with respect to the interferometer's zero-phase delay after the fast Fourier transform (FFT) process, such that only half of the depth range can generally be used.

To extend the imaging depth, various full range methods have been introduced. As a well-known method, the phase shifting method [6,7] can retrieve a complex image from a few frames of interference fringes obtained using the different phases of a reference beam. Furthermore, BM-mode scanning [8] simultaneously uses phase modulation of the reference beam (M-scan) and sample scanning (B-scan). The reference scanning-free phase shift method was also developed, which uses the off-axis galvano scan in the sample arm [9]. However, development of a full range probe-based system has not similarly progressed like as a system equipped with a bulk sampling arm, though it could potentially improve the image contrast for human tympanic membranes and organs. Until now, only a few full range endoscopic OCT systems have been reported [10].

In this Letter, we propose the development of a full range SD-OCT using a fiber-optic scanning probe. For full range, we adopted the BM scan technique. Since a fiber-optic probe scans like a free-standing cantilever, the light emanating from the fiber tip follows an arc line in the direction of the fiber's tip angle. Then, unintentional phase shift occurs, though this phase shift is not sufficient for full range processing, so we also tilted the fiber. As a result, a complex-conjugate-free OCT image was obtained

with no modification in the probe configuration. To realize this probe, we constructed SD-OCT system and a magnetically actuated fiber-optic probe [4]. The fiber-optic probe-based complex SD-OCT system is shown in Fig. 1.

A broadband light source having a center wavelength of 840 nm and a spectral bandwidth of 62 nm was used. The measured axial resolution was 8 μm . The confocal parameter was 0.37 mm at a lateral resolution of 14 μm . The light was split into reference and sample beams by using an optical coupler. Here, a probe actuated by a magnetic force was employed in order to achieve sample scanning, which also served to phase shift the complex SD-OCT. Figures 2(a) and 2(b) show a schematic of the probe and a photograph of the implemented probe under a scanning motion.

The beam backscattered from the sample creates an interference pattern with the reference beam reflected at the reference mirror. The 2D spectral interference signal detected with a line CCD is expressed as

$$I(\omega, t) = I_R(\omega) + I_s(\omega, t) + 2[I_R(\omega)I_s(\omega, t)]^{1/2} \times \cos(\Delta\varphi_s(\omega, t) + \varphi(t)), \quad (1)$$

where ω and t are the optical angular frequency and time, respectively. In addition, $I_R(\omega)$ and $I_s(\omega, t)$ are the light intensities of the reference and sample beams,

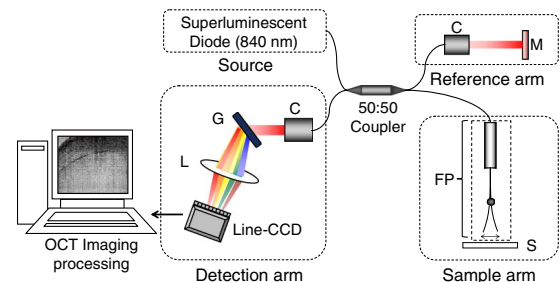


Fig. 1. (Color online) Schematic of a full range SD-OCT system based on a fiber-optic probe. C, collimator lens; M, mirror; L, lens; G, grating; FP, fiber-optic probe; S, sample.

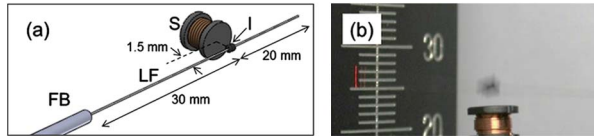


Fig. 2. (Color online) (a) Schematic of the probe. The probe can be subdivided into two major parts: lensed fiber and solenoid-based actuator. (b) Photograph of scanning motion. He-Ne laser at 635 nm was used to visualize the scanning motion. S, solenoid; I, iron-bead; LF, lensed fiber; FB, fixed bar.

$\Delta\varphi_s(\omega, t)$ is the time-dependent phase delay of the sample beam against the reference beam, and $\varphi(t)$ is the time dependent phase offset that occurs during scanning. In this Letter, we show that a fiber-based scanner can be used to change the $\varphi(t)$ term for a full range complex OCT image.

Figure 3 presents a schematic of the scanning motion of the probe, and a photograph taken during a single lateral scan, corresponding to the red box in Fig. 3(a). Note that Fig. 3(a) is slightly exaggerated to assist in understanding the concept of phase offset in the probe. In the figure, the green line denotes a lensed fiber whose real shape is shown in the inset of Fig. 3(b); it simply comprises a single mode fiber (SMF), coreless silica fiber (CSF), and lens. The lensed fiber is fixed at one point, like a free-end cantilever, and the fixed point in the figure indicates the rigidly fixed end of the fiber. The other end of the fiber piece is actuated with a scan angle θ_s and a tilt angle θ_t . To realize the tilt angle, we simply tilted the fiber itself while scanning. The introduced tilt angle had only a positive (or negative) value for the time derivative of the phase offset, which avoided image flipping, and also provided a sufficient spatial frequency shift after performing FFT in a lateral direction. The photograph in Fig. 3(b) was taken with a digital camera during scanning, and the He-Ne laser emanating from the lensed fiber shows the scanning track. If we assume that a

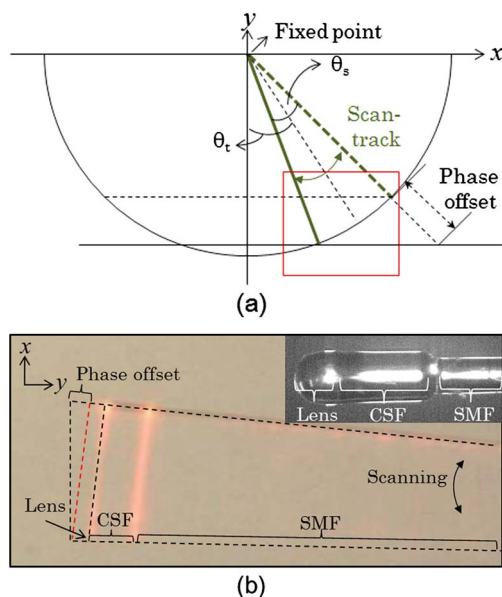


Fig. 3. (Color online) (a) Schematic diagram and (b) photograph of fiber end, illustrating the concept of phase offset in a fiber-based scanner. θ_s , scan angle; θ_t , tilt angle.

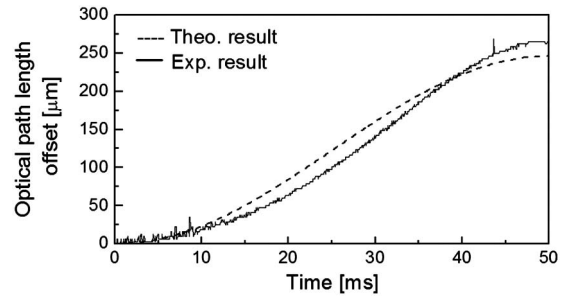


Fig. 4. Graph of optical path length offset of theoretical result (dotted curve) and experimental result (solid curve) with respect to time.

sample is placed horizontally (x direction), the phase offset can be determined as shown in Fig. 3(a).

While lateral scanning, the optical path length offset (μm) with respect to time is theoretically and experimentally illustrated in Fig. 4. Note that though the two results are not exactly the same, they are well matched. The results were obtained for θ_s and θ_t at about 3.5° and 4.5° , respectively, and a scan range of about 3 mm.

In our experiment, the number of A-lines per each B-scan is 1200 and the maximum optical path length offset was calculated as $246 \mu\text{m}$ to ensure that a sufficient spatial frequency shift is provided. Furthermore, the separation between A-lines is about $1/5.6$ of the spot size of the beam, which is an important factor due to the mirror term suppression ratio [9].

Figure 5 shows the flow diagram of the full range image reconstruction procedure. First, a two-dimensional (2D) spectral interferogram was obtained for a single B-scan [Fig. 5(a)]. In the lateral direction, phase is non-linearly changed, as in Fig. 4. Using this phase change, the BM scan technique [8] was applied for a fiber-based

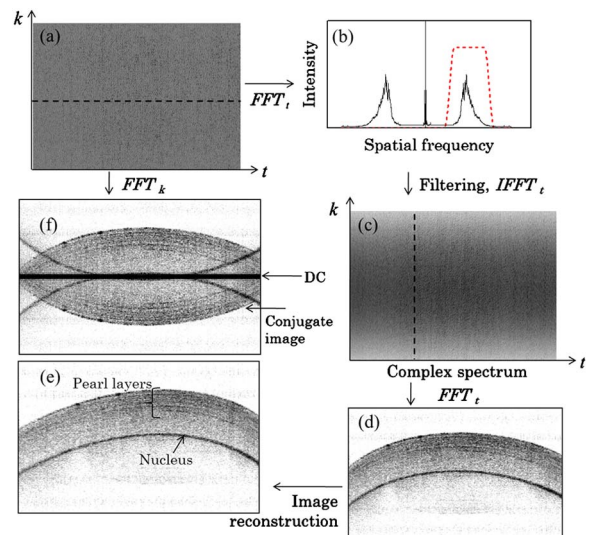


Fig. 5. (Color online) Flow diagram of full range image reconstruction process: (a) 2D spectral interferogram, (b) result of FFT of spectral interferogram in the lateral direction (dotted red curve indicates spatial frequency filter), (c) complex spectrum obtained after filtering and inverse FFT of (b), (d) full range image after FFT of complex spectrum in the optical wavenumber domain, (e) reconstructed full range image considering fiber motion, and (f) standard overlapping SD-OCT image.

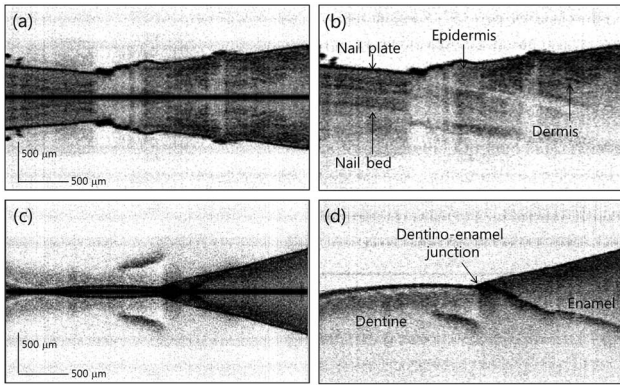


Fig. 6. Full range SD-OCT images of biological samples: (a) standard OCT image and (b) full range image of human fingernail near the nail fold region; (c) standard OCT image and (d) full range image of a human tooth near the dentino-enamel junction.

scanner in order to obtain a full range image. Then, the interferogram of Fig. 5(a) was fast Fourier transformed in the lateral direction. Figure 5(b) presents the FFT results for a single lateral line of Fig. 5(a) (dotted black line); then, only the positive/negative complex conjugate signal was selected, using the spatial frequency filter shown by the dotted red curve. However, since the phase offset changes nonlinearly, the signal peak of the FFT result becomes broad, so image information can be lost after filtering. To avoid this problem, prior to the FFT process, we resampled the phase so that phase can change linearly. Subsequently, the phase interval between two adjacent A-lines became $\pi/2$ rad. The complex spectrum [Fig. 5(c)] was obtained after the inverse FFT of the filtered signal. Next, the FFT was performed again, but in the optical wavenumber k domain. As a result, we obtained the full range image shown in Fig. 5(d), and as the last step, the image was reconstructed, since the fiber scans sinusoidally over time [Fig. 5(e)]. Without the above process, we would obtain an overlapping image such as that in Fig. 5(f), which also has a strong dc term. The images in Figs. 5(d)–5(f) are of a pearl that has several layers inside and a nucleus.

To verify the usability of this technique, we also imaged several biological samples. Figures 6(a) and 6(b) are in vivo SD-OCT images of a human fingernail near the nail fold region. Each image was obtained without and with the full range imaging process. In Fig. 6(a), the desired image is overlapped with a conjugated image using dc and an autocorrelation signal; therefore, the real signal is difficult to distinguish. In contrast, in Fig. 6(b), we can easily see nail structures such as the nail plate, nail bed, epidermis, and dermis. Figures 6(c) and 6(d)

are SD-OCT images of a human tooth taken without and with the full range imaging process. In Fig. 6(d), structures of the dentine, enamel, and dentino-enamel junction are clearly identified. Note that the physical size of both images is $2.3 \text{ mm} \times 3 \text{ mm}$ (depth \times lateral, $648 \text{ pixels} \times 1200 \text{ pixels}$), and the acquisition speed is 20 frames/s.

In summary, we presented a full range SD-OCT method using a fiber-based scanning probe. Due to the nonlinear scanning motion of the cantilever fiber, the phase offset could continuously change over time. However, to void image flipping and nonfrequency shift region and also to provide sufficient spatial frequency shift, we supplied an additional tilt angle to the fiber axis. Thus, the phase shift was achieved during the sample scanning. With the suggested technique, the full range complex-conjugate-free SD-OCT images of a pearl, human fingernail, and human tooth could be successfully acquired. By further developing this method, it is expected that a high sensitivity endoscopic probe can be realized for biomedical imaging in the future. In addition, though the current probe is still too big for clinical applications, we can reduce the size of the driving coil by simply using a thin but strong ferromagnetic rod or wire having high magnetic permeability as the solenoid core.

This study was supported by a grant of the Korean Health Technology R&D Project, Ministry for Health, Welfare & Family Affairs, Republic of Korea (No. A100490).

References

1. D. Huang, E. A. Swanson, C. P. Lin, J. S. Schuman, W. G. Stinson, W. Chang, M. R. Hee, T. Flotte, K. Gregory, C. A. Puliafito, and J. G. Fujimoto, *Science* **254**, 1178 (1991).
2. A. F. Fercher, C. K. Hitzenberger, G. Kamp, and S. Y. El-Zaiat, *Opt. Commun.* **117**, 43 (1995).
3. Z. Yaqoob, J. Wu, E. J. McDowell, X. Heng, and C. Yang, *J. Biomed. Opt.* **11**, 063001 (2006).
4. E. J. Min, J. Na, S. Y. Ryu, and B. H. Lee, *Opt. Lett.* **34**, 1897 (2009).
5. T. Tsai, B. Potsaid, M. F. Kraus, C. Zhou, Y. K. Tao, J. Hornegger, and J. G. Fujimoto, *Biomed. Opt. Express* **2**, 2438 (2011).
6. M. Wojtkowski, A. Kowalczyk, R. Leitgeb, and A. F. Fercher, *Opt. Lett.* **27**, 1415 (2002).
7. R. A. Leitgeb, C. K. Hitzenberger, A. F. Fercher, and T. Bajraszewski, *Opt. Lett.* **28**, 2201 (2003).
8. Y. Yasuno, S. Makita, T. Endo, G. Aoki, M. Itoh, and T. Yatagai, *Appl. Opt.* **45**, 1861 (2006).
9. R. A. Leitgeb, R. Michaely, T. Lasser, and S. C. Sekhar, *Opt. Lett.* **32**, 3453 (2007).
10. K. Zhang, Y. Huang, and J. U. Kang, *Opt. Eng.* **50**, 119002 (2011).